Quasi-Periodicity at Transition from Spiking to Bursting in the Pernarowski Model of Pancreatic Beta Cells

Haniyeh Fallah[1]* and Andrey L. Shilnikov[2]**

[1] Department of Mathematics and Computer Science, Amirkabir University of Technology, 15875-4413 Tehran, Iran

[2] Department of Mathematics and Statistics, Georgia State University, 100 Piedmont Ave, 30303 Atlanta, USA

Abstract—This paper studies quasi-periodicity phenomena appearing at the transition from spiking to bursting activities in the Pernarowski model of pancreatic beta cells. Continuing the parameter, we show that the torus bifurcation is responsible for the transition between spiking and bursting. Our investigation involves different torus bifurcations, such as supercritical torus bifurcation, saddle torus canard, resonant torus, self-similar torus fractals, and torus destruction. These bifurcations give rise to complex or multistable dynamics. Despite being a dissipative system, the model still exhibits KAM tori, as we have illustrated. We provide two scenarios for the onset of resonant tori using the Poincaré return map, where global bifurcations happen because of the saddle-node or inverse period-doubling bifurcations. The blue-sky catastrophe takes place at the transition route from bursting to spiking.

1. INTRODUCTION

We are sincerely grateful to the Editors who curated this special issue dedicated to the 70th and 80th birthdays of two exceptional mathematicians, S. V. Gonchenko and V. N. Belykh. One of us, A. L. S., has had the honor of knowing both personally and professionally for an extended period of fast-flying time.

Sergey Gonchenko has emerged as a rightful leader and scientific authority within the L. P. Shilnikov school of bifurcations in dynamical systems with complex chaotic dynamics.

Vladimir Nikolaevich Belykh truly stands as "the last of the Mohicans" of the Gorky school of dynamical systems and oscillations. A. L. S. expresses deep gratitude to him for his wisdom, unwavering support, and for being a role model of a distinguished academician, as manifested by his long and unique trajectory in research and mentoring.

Pancreatic beta cells produce and secrete insulin to regularize the blood glucose level [1–5]. Beta cells display bursting oscillations in the presence of glucose. Bursting are oscillatory rhythms where some variable alters between silent and active phases. The active phase experiences rapid oscillation of the membrane potential, in contrast to the silent phase, where slow changes occur.

---

*E-mail: hfallah@aut.ac.ir

**E-mail: ashilnikov@gsu.edu

Many biophysical models are proposed to describe oscillatory activities in these cells, e. g., Chay – Keizer [2] and Sherman – Rinzel – Keizer (SRK) models [5]; see [6, 7] for a review of the mathematical modeling of beta cells. The equations of the biophysical models being complicated, the researchers developed circuit analog models to better analyze the oscillatory dynamics. The Pernarowski system, a simple polynomial model, is such an analogous system to the biophysical models describing the oscillatory dynamics of beta cells. In the same way, the Fitzhugh – Nagumo model [8] is an analogous model to the Hodgkin – Huxley system explaining the oscillatory activities in the squid giant axon, and the Hindmarsh and Rose system [9] is analogous to the Plant-Kim model explaining the bursting activities of the Aplysia neuron. The simplicity of the polynomial functions used in analog models allows much of their analysis to be done through analytical means. The analog models have fewer dependent variables and parameters than the corresponding biological models.

This paper examines the Pernarowski system dynamics as it relates to the process of transitioning from spiking to bursting. The model has already been studied by the authors in [10]. They analyzed its fast subsystem bifurcations across various parameters. In that study, the goal was to expect possible bursting types using Izhikevich's classification method. This method categorizes burst activity according to the bifurcations that start and end rapid spiking, returning to the initial resting state [11, 12]. In an earlier study, the authors showed the period-doubling cascades of canards as the mechanism describing the transition from spiking to bursting in this model [13]. The Pernarowski system has not been examined for global bifurcations that result in the shift between oscillatory types. This paper investigates global bifurcations leading to multiple quasi-periodicity oscillations, self-similar torus fractals, and multistability in the Pernarowski model. The classification of the oscillatory patterns transitions is a basic problem in dynamical systems theory and neuroscience. More complex bifurcation structures are observed in the transition route from bursting to spiking, especially in neuronal systems [13–16]. Such bifurcations include, e. g., homoclinic bifurcations [17–19], torus canard [20], torus break-down [21–23], and blue-sky catastrophe [24–28]. There exists an incomplete explanation of the possible transitions between oscillatory rhythms.

We show that a saddle torus canard causes the transition between bursting and spiking. During the spiking window, the stable periodic orbit is surrounded by resonant tori because of global bifurcations of saddle-node (fold of periodic orbit) or inverse period-doubling. The number and topology of torus orbits are varied by adjusting the system parameters. Some intriguing situations present the coexistence of several resonant tori with distinct periods. In the presence of several attractors, the Pernarowski system exhibits multistability for the same parameter values that are affected by changes in initial conditions. There is a competition among the attractors to define their basin of attraction. In some situations, Kolmogorov – Arnold – Moser (KAM) tori [29] enclose the stable periodic orbit.

KAM tori appear frequently in integrable Hamiltonian systems. KAM theory studies the persistence of these quasi-periodic oscillations in integrable Hamiltonian systems subjected to perturbation [30, 31]. Here, the main question is to determine the fate of these quasi-periodic solutions with a perturbation in the structure of Hamilton's equations. Specifically, they will be destroyed or survive, becoming deformed. Kolmogorov [32] showed that, for near-integrable systems, almost all quasi-periodic oscillations persist as invariant KAM tori. However, the quasi-periodic trajectories on the resonant tori are less robust to survive rather than those on the nonresonant tori. The existence of KAM tori in dissipative systems is seldom reported in the literature. Since the fast subsystem of the Pernarowski system is integrable [33], this model can show KAM tori despite being a dissipative system. Here, we prove that this is the case and this system exhibits KAM tori surrounding the spiking periodic orbit.

We demonstrate that certain situations exhibit a self-similar phenomenon, revealing fractals near the saddle torus canard, where the dynamical regime around each stable periodic orbit on the resonant torus is like the original one. Parameter variation causes the spiking periodic orbit to lose stability and transits to an ergodic torus. The torus starts out smooth, but becomes nonsmooth as it approaches the saddle orbit on the surrounding torus. Then it breaks down by a homoclinic bifurcation.

The time scale disparity between ion channels leads to beta cell activities being described as fast-slow systems. Trajectories in fast-slow systems are close to slow-motion manifolds most of the

time. There are two such manifolds in cell models: quiescent (M_{eq}) and tonic spiking (M_{po}). The quiescent manifold makes up the equilibrium states of the system, and the spiking one comprises its periodic solutions. Bursting activity is associated with a solution that switches between these manifolds. The system solution spiraling around M_{po} without visiting the quiescent phase relates to the continuous spiking, which may be periodic or aperiodic.

We point out that the slow-motion manifolds are specified without decomposing the fast-slow system. Using the decomposition method, the singular limit $\varepsilon = 0$ freezes the slow variable as the control parameter of the fast subsystem to continue the critical manifolds of equilibria and periodic orbits. The slow-fast decomposition of the system cannot explain the variety of observed dynamics resulting from new bifurcations in the full model such as the blue-sky catastrophe [27]. In [19], the authors used the slow-motion manifolds of the full system as an alternative approach instead of the fast subsystem [26–28]. In this technique, the slow-motion manifolds are attained by selecting a suitable slow parameter and continuing it rather than the slow variable [19]. The critical point of the full system is achieved when the equilibria manifold intersects with the slow nullcline. Using an averaging technique, we can predict the place of spiking periodic orbits on the tonic-spiking manifold.

The oscillatory character of the bursting activities and tonic spiking makes a compelling case for the use of the Poincaré return mappings to reveal the mechanisms of transitions between activity types. The Poincaré return map is a useful tool to study the dynamics near the tonic-spiking manifold. The successive maximum of the voltage variable will construct the Poincaré map. First, we determine the spiking manifold in the phase-space of the system. We follow the branch of the periodic orbits, continuing a control parameter applying a parameter continuation technique that yields a parametric foliation of the aforementioned manifold by many periodic orbits. Next, we determine the maximum of the voltage variable on each periodic orbit that is used as an initial phase point for integrating the solution. Then we follow the next maximum of the voltage.

The paper is organized as follows: first, we introduce the Pernarowski model in Section 2. In Section 3, we describe the phase space of the model and its bifurcations. In Section 4, we study the bifurcations of resonant tori. The focus of our discussion is the self-similarity of dynamical regimes inside the resonant torus. In Section 5, we investigate the mechanism of torus break-down. In Section 6, we discuss another scenario for the torus bifurcation that takes place near the fold of the tonic-spiking manifold. We summarize the results in the conclusion section.

2. THE PERNAROWSKI MODEL OF A BETA CELL

A general model describing the activity of a single beta cell (see [34] and references therein) can be written as

$$C\frac{du}{dt} = -\sum_k I_k(u, v, \mathbf{z}), \tag{2.1a}$$

$$\frac{dv}{dt} = \frac{v_\infty(u, \mathbf{z}) - v}{\tau(u, \mathbf{z})}, \tag{2.1b}$$

$$\frac{d\mathbf{z}}{dt} = \varepsilon\mathbf{h}(u, v, \mathbf{z}), \quad \text{where} \quad \mathbf{z} \in \mathbb{R}^n. \tag{2.1c}$$

Here, C is the cell membrane capacitance, the dynamic u-variable represents the membrane potential, I_k stands for an ionic current flowing through a k-type channel across the cell membrane, the v-variable represents the activation probability of the potassium channel, and ε is a small parameter. The vector $\mathbf{z}$ defines the condensation of agents such as an intracellular calcium, and the calcium in the endoplasmic reticulum to regulate the bursting electrical activity in the model. Note that the last equation in the system (2.1) describes the calcium dynamics, which varies slowly due to small ε. Depending on what hypotheses were made while deriving the model equations, different forms can be defined for the nonlinear functions in Eqs. (2.1) above. Some other models of a single beta cell can be also formalized as follows:

$$\dot{u} = f(u) - v - g(z), \tag{2.2a}$$

$$\dot{v} = \frac{v_\infty(u) - v}{\tau_\infty(u)}, \tag{2.2b}$$

$$\dot{z} = \varepsilon H(u, c) = \varepsilon(\beta h(u) - z), \tag{2.2c}$$

where $\varepsilon \ll 1$ is a singular parameter, while β is a finite constant. The nonlinear functions $g(z)$, $f(u)$, $\tau_\infty(u)$, $v_\infty(u)$, and $H(u, z)$ in system (2.2) can be calibrated to describe various channel conductances and ionic currents in each specific model depending on its biological interpretation. Here, the dynamic variable u defines the membrane potential as above, and z describes the intracellular concentration of agents related to calcium ions that regulate the bursting activities in the cell and its model. Equations (2.2) can be further transformed into the following Lienard form by differentiating the u-variable twice and thus eliminating v as follows:

$$\ddot{u} + F(u)\dot{u} + G(u, z) = \varepsilon g'(z) H(u, z), \tag{2.3}$$

where

$$F(u) = \frac{1}{\tau_\infty(u)} - f'(u), \tag{2.4a}$$

$$G(u, z) = \frac{1}{\tau_v(u)} \big(v_\infty(u) + g(z) - f(u)\big). \tag{2.4b}$$

Commonly, the beta cell literature examines Eq. (2.3) rather than Eqs. (2.2) since the term $F(u)\dot{u}$ turns out to become small in models featuring bursting activity, and therefore it can be omitted. Both model representations were studied in [35] in the particular case referred to as a P_{lmn}-model, where the functions $F(u)$, $G(u, z)$, and $H(u, z)$ were defined as polynomials in the u-variable of degrees l, m, and n, respectively. Here, we present our study of a specific P_{231}-model known as the Pernarowski model [10] in which those polynomials (as indexed by p) are given by

$$F_p(u) = a\big((u - \hat{u})^2 - \eta^2\big), \tag{2.5a}$$

$$G_p(u, z) = z + u^3 - 3(u + 1), \tag{2.5b}$$

$$H_p(u, z) = \beta(u - \bar{u}) - z, \tag{2.5c}$$

with the parameter vector $\lambda = (a, \eta, \hat{u}, \beta, \bar{u}, \varepsilon)$. The Pernarowski system is defined as

$$\ddot{u} + F_p(u)\dot{u} + G_p(u, z) = \varepsilon H_p(u, z). \tag{2.6}$$

The fast subsystem in equation (2.6) can be obtained by setting $\varepsilon = 0$ in the singular limit. This lets us define the parameters a, η, and $\hat{u}$ as fast ones as they belong to the fast system only, whereas we will refer to $\bar{u}$ and β as slow variables. The biological meaning of the slow parameters has to do with the glucose level in the beta cell; dynamically, their variations make the corresponding model switch its activity behaviors, including tonic-spiking, bursting, and nonoscillatory activity. In this study, we assume that the parameters $(a, \hat{u}, \beta, \epsilon) = (0.02, 0, 4, 0.005)$ remain fixed, respectively.

3. PHASE SPACE AND BIFURCATION ANALYSIS

To explain the bifurcations revealing different oscillatory types in the Pernarowski model, we can use the geometric fast-slow decomposition, as depicted in Fig. 1. The decomposition relies on dissecting the dynamics into fast and slow sections. In our system, the variable z is the slow variable, while the others are fast. Figure 1 illustrates the (u, y, z) phase space projection for fixed $\eta = 1.2$, showing bursting and tonic spiking orbits superimposed in the slow-motion manifolds: 2D tonic-spiking manifold M_{po} and 1D quiescent curve M_{eq}. The quiescent manifold is an S-shaped curve that has saddle points in the middle and stable points in the upper and lower segments. A stable limit cycle on M_{po} that is created by a Hopf bifurcation loses its stability through a torus bifurcation and collides with a saddle point via a homoclinic to the saddle point after experiencing a period-doubling bifurcation. A similar manifold takes place near the right knee, which endows the

model with another hysteresis that generates symmetric and asymmetric bursting oscillations. The existence and location of the torus and successive period-doubling (flip) bifurcations, as reported in [36], represents the physiological bounds of ion gradient variation that can cause significant alterations in spiking oscillations frequency and structure.

To create the slow-motion manifolds, we use a parameter continuation approach to detect equilibria and the periodic orbits of the system. We use $\bar{u}$ as the primary bifurcation parameter since it is the offset of u, which affects only the slow variable z. Varying $\bar{u}$ shifts the slow nullcline $z' = 0$ in the phase space, as a result, the crossing point between the equilibrium curve (M_{eq}) and the slow nullcline shifts to achieve the tracing of M_{eq}. We could trace the other manifold M_{po} by following the same method described in [19]. We note that a new method is being used to localize slow-motion manifolds. The conventional decomposition method follows the equilibria or tonic-spiking manifolds by freezing the slow variable as the control parameter. The essence of the new method lies in the application of the parameter continuation technique to the full model equations instead of the fast subsystem. This method has the advantage that it directly produces the desired manifolds rather than just those of the fast subsystem, which supplements the conventional method without neglecting the slow dynamics. Multiple time scales in high-dimensional models make the dissection method problematic, which is where this method becomes precious. This method can detect and describe nonlocal bifurcations that are due to reciprocal interactions of fast and slow dynamics.

We will exhibit the multistable nature of the model, which includes a small spiking window, resonance torus states, and bursting oscillations. Different states are identified as the slow nullcline moves with the alteration of the parameter $\bar{u}$. The system undergoes tonic spiking when it has a stable periodic orbit on M_{po}. When the slow nullcline $z' = 0$ does not cross the stable parts of M_{po} and M_{eq} manifolds, the system shows bursting behavior and both manifolds become transitive. A system variable changes between a silent phase on a branch of M_{eq} and an active state on the tonic-spiking manifold M_{po} to represent bursting. The number of spikes per burst is determined by the rotations around each branch of M_{po}. Longer burst duration implies a large revolution number. The slow-motion manifolds in Fig. 1 exhibit a symmetric bursting. During symmetric bursting, a variable in a system will visit two silent and active phases before returning to its start state. At the same saddle point, we can see two homoclinic bifurcations in Fig. 1. Large amplitude spiking rhythms appear per each burst, as the slow-nullcline crosses the average curves at the same saddle point (e. g., at $\bar{u} \simeq -0.7$). The mixed-mode rhythms have both bursting and spiking oscillations. As the revolution number increases, the system continues spiking at $\bar{u} = -0.73$. Also, the transition between bursting and spiking in the Pernarowski model exhibits a blue-sky catastrophe. We will review this in the upcoming sections.

We use a bifurcation diagram to show how spiking transits to bursting by changing the parameters $\bar{u}$ and η. Here, $\bar{u}$ is the main parameter that changes fixed points and periodic orbit positions by altering the slow nullcline. In Fig. 2, the yellow curves show Andronov–Hopf (AH) bifurcations with a critical point labeled GH. The criticality means that either an unstable or a stable limit cycle appears. It collapses into the critical point, passing through the corresponding portion of the AH-curve. Bautin was the first to study this bifurcation and found out that it involves a saddle-node of the limit cycle bifurcation. This happens when the saddle and stable limit cycles merge from subcritical and supercritical Hopf bifurcations. The saddle-node of the limit cycle bifurcation is the so-called fold bifurcation. It happens on the tonic-spiking manifold, determined by the limit cycles of the full system using parameter continuation. When a fold bifurcation is reached, a spiking periodic-orbit can turn into bursting through a torus or period-doubling bifurcations. A torus can occur when passing from tonic-spiking to bursting because of the fold bifurcation from the Bautin point. The authors of [22] have reported evidence of this phenomenon in the Purkinje cell model. The Pernarowski model exhibits this phenomenon as well.

Continuing $\bar{u}$ at each fixed η value starts the tonic-spiking manifold from the Andronov–Hopf bifurcation point. The manifold ends either with a homoclinic bifurcation at each fixed value of η between 0 and 1.4 or with fold bifurcations between 1.4 and 1.7. After that, it finishes at the right Andronov–Hopf bifurcation. See Fig. 2. The system dynamics are symmetric near the knees. There
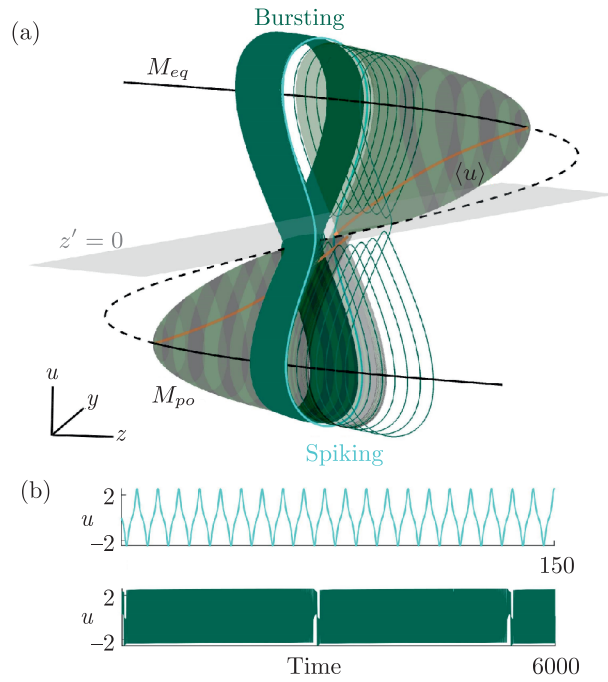
Fig. 1. (a) 3D phase space of the Pernarowski system at $\eta = 1.2$ achieved by continuing $\bar{u}$. Slow-motion manifolds include 1D quiescent M_{eq} made of equilibria of the model, and 2D tonic-spiking M_{po} spanned by its periodic orbits. Both branches, top and bottom, of M_{po} terminate at the homoclinic saddle at the origin on M_{eq} through which the slow nullcline (grey surface) labeled as $z' = 0$ passes. The model is bistable as it can exhibit symmetric mixed-mode oscillations composed of alternating bursting or coexisting periodic spiking ones. (b) Time series corresponding to the tonic spiking oscillations and mixed-mode bursting of the matching colors.
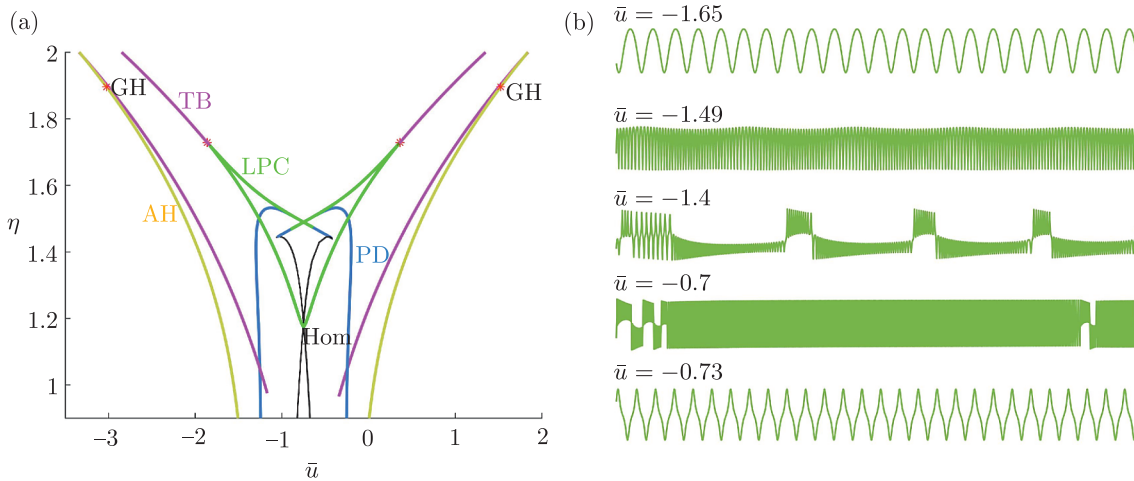

Fig. 2. Dynamical regimes of the Pernarowski model. (a) The $(\bar{u}, \eta)$-bifurcation diagram including the Andronov–Hopf (AH) bifurcation curves (yellow) with codimension-2 Bautin points (GH). The purple lines correspond to the torus bifurcations (TB); the blue ones correspond to period-doubling (PD) bifurcations, while the green lines labeled by LPC and originating from the symmetric cusps indicate the saddle-node (fold) bifurcations of periodic orbits, whereas the black lines (Hom) correspond to homoclinic bifurcations. (b) Evolution of oscillatory patterns with increasing $\bar{u}$-values at fixed $\eta = 1.2$.

are two sets of torus bifurcations labeled TB (purple curves). First one starts in the fold bifurcations at $\eta \simeq 1.7$ and continues for higher η values. The second set splits off from the curves labeled AH at the GH points. The periodic orbit born at the supercritical Hopf point loses stability through either a torus bifurcation or a period-doubling one. The type of bifurcation would be expected by

the nonlocal properties of the flow: when the phase space volume contracts, the tonic spiking limit cycle can undergo a period-doubling bifurcation. Otherwise, it undergoes a torus bifurcation. In the region enveloped by AH and TB lines, a variety of states might appear. Such states include stable periodic orbits, resonant tori, self-similar torus fractals, KAM tori, and large amplitude bursting oscillations.

The small spiking window separates from the bursting state via a saddle torus canard, wrapping the periodic orbit. Inside the spiking window, multiple resonant tori emerge through saddle-node or inverse period-doubling bifurcations. There are situations where the system is bistable between bursting and tonic-spiking where both states can be generated by the model relying on initial conditions, as depicted in Fig. 3 on the $\eta = 1.4$ pathway at $\bar{u} = 0.32$. The saddle torus canard is responsible for the system transitioning to bursting. A basin of attraction of the spiking state is surrounded by the saddle torus that separates it from that of the bursting state. The same bistability is also seen in the FitzHugh – Nagumo – Rinzel model, the Purkinje cell model, and parabolic burster models [22].
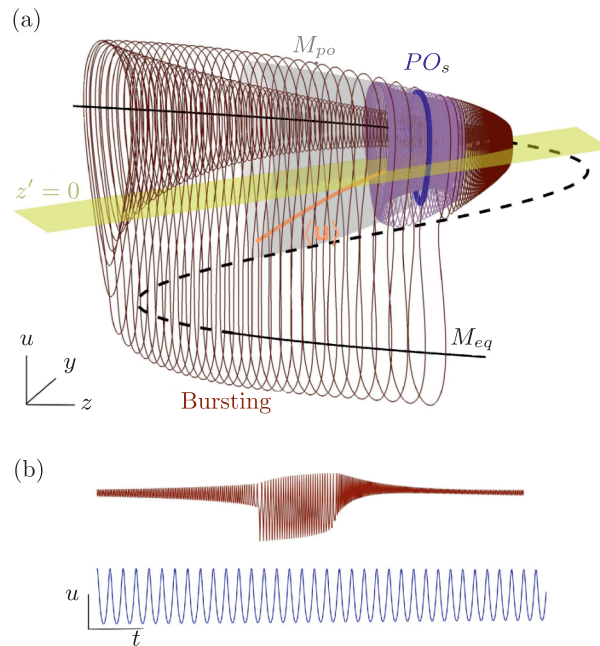
Fig. 3. (a) Phase space projection illustrating the bistability in the model at $\eta = 1.4$ and $\bar{u} = 0.32$ where the basin of a stable spiking periodic orbit PO_s is bounded by a repelling saddle torus canard (purple orbits) from that of a coexisting bursting one (shown in brown) near the slow-motion manifold M_{po}. The orange line is the average curve of M_{po}, whose intersection with the slow nullcline $z' = 0$ finds the location of the periodic orbit. (b) Time series of bursting and spiking orbits.

Quasi-periodic oscillations replace the small spiking window when the periodic orbit becomes unstable through a torus bifurcation. Multiple quasi-periodic oscillations, along with bursting oscillations, create a multistable model that is influenced by an ergodic torus and several resonant tori. The transition to bursting is also caused by a saddle torus canard. We examined this scenario in the $\eta = 1.4$ pathway at $\bar{u} = 0.29$, where the tonic-spiking limit cycle loses its stability to form a 2D torus through a supercritical torus bifurcation. It separated a small basin of attraction of the born torus from that of bursting through a saddle torus, as illustrated in Fig. 4. We have examined the torus stability by tracking the stable state of the system by varying the initial value of $u \in (2.07, 2.08)$ at fixed $y = -0.5158$, $z = 3.8337$. Simulations were long enough under each initial condition to achieve some steady states. We then displayed the stable states by maximal values of the variable u, as shown in Fig. 4c. The phase portrait, trajectories, and the Poincaré map relating to the two stable states and the dividing saddle torus are illustrated in Figs. 4a–4c. Also, the corresponding time series is shown in Fig. 4d.
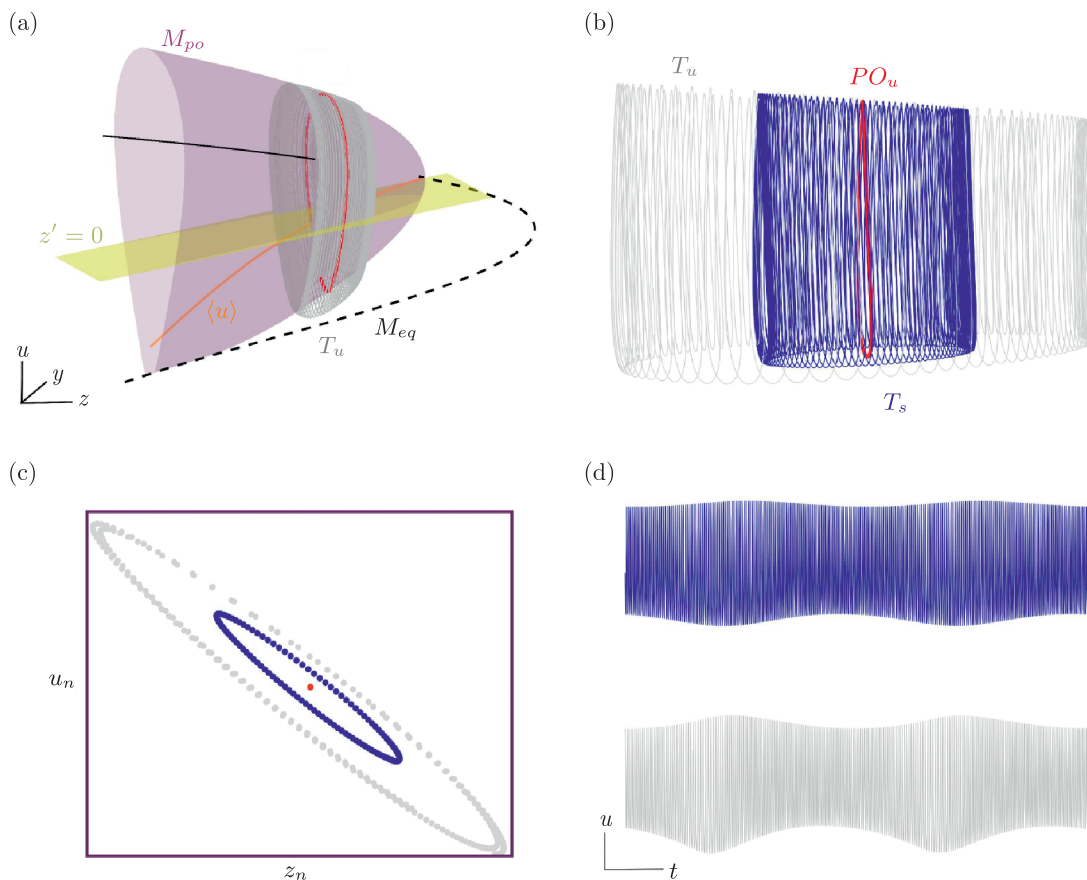
Fig. 4. (a) 3D phase space at $\eta = 1.4$ showing the slow-motion manifolds including the tonic-spiking manifold M_{po} with an unstable periodic orbit PO_u at the location of the torus bifurcation and the saddle torus superimposed on it, as well as the quiescent manifold M_{eq} with unstable (dashed) and stable (solid) portions divided by the supercritical Hopf bifurcation. The yellow surface $z' = 0$ is the slow nullcline, whose intersection with the average curve $\langle u \rangle$ finds the location of PO_u on M_{po}. (b) 2D saddle torus (grey, T_u) surrounding the stable torus (blue, T_s) enclosing the unstable periodic orbit (red point PO_u) at $\bar{u} = 0.29$. (c) The Poincaré map depicting the maxima of each tori corresponding to inset (b). (d) Time series of each tori in (b).

4. QUASI-PERIODICITY THROUGH A RESONANT TORUS

Figure 5 shows a 1:3 resonant torus with a pair of limit cycles, stable and saddle, superimposed on it. The torus surrounds a stable periodic orbit. A saddle torus canard is present around it. The stable periodic orbit on the resonant tori is determined by the filled nodes on the Poincaré map. Unfilled nodes relate to the saddle torus canard. A small basin of attraction of the stable periodic orbit on the torus achieves quasi-periodicity oscillations. Bursting with high amplitude and symmetry can occur beyond the saddle torus canard. Leaving the saddle periodic orbit on the torus can lead to the appearance of small periodic oscillations.

Saddle-node or inverse period-doubling bifurcations result in a resonant torus near the saddle torus canard. Figure 6 shows the $(u, y, z)-$phase space projection at $\eta = 1.102$ with the stable periodic orbit (blue curve), quasi-periodicity (light blue curve), and the saddle torus canard (red curve) superimposed on the slow-motion manifolds at $\bar{u} = -1.35011$. The resonant torus contains a quasi-periodic orbit with a period of 11, which was discovered earlier through a sequence of inverse period-doubling bifurcations ($\bar{u} = -1.351378$). At $\bar{u} = -1.35002847$, a saddle-node bifurcation will cause the torus to vanish. Figure 6d shows Poincaré return maps of the periodic orbit and the invariant tori on a cross-section, defined on maximum values of u by continuing a small range of initial values to reveal the dynamics. The stable periodic orbit on the stable torus corresponds to the blue period-11 points. Observe the stable fixed point marked in blue at the center of the diagram, with blue and red period-11 points around it that correspond to stable and saddle
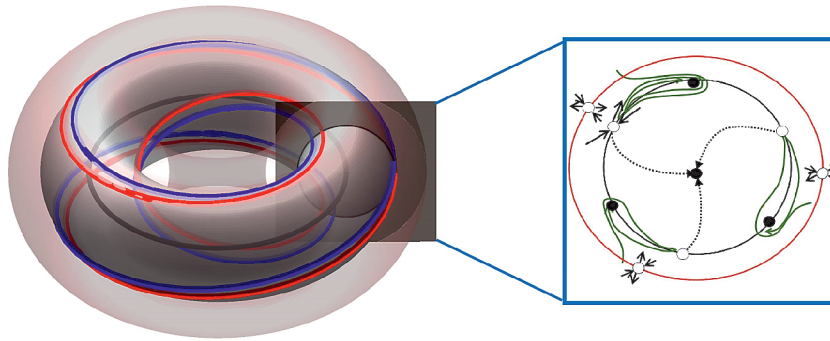
Fig. 5. An illustration of a saddle torus canard surrounding a 1:3-resonant torus with a pair of periodic orbits, stable and saddle, on it that correspond to stable and saddle period-3 points in the Poincaré return map on a cross-section transverse to the tori.

orbits, respectively, in the 3D phase space. Here, grey lines connect successive iterates, turning counterclockwise in the return map. The torus moves away from the saddle torus canard and vanishes through a saddle-node bifurcation as $\bar{u}$ increases.
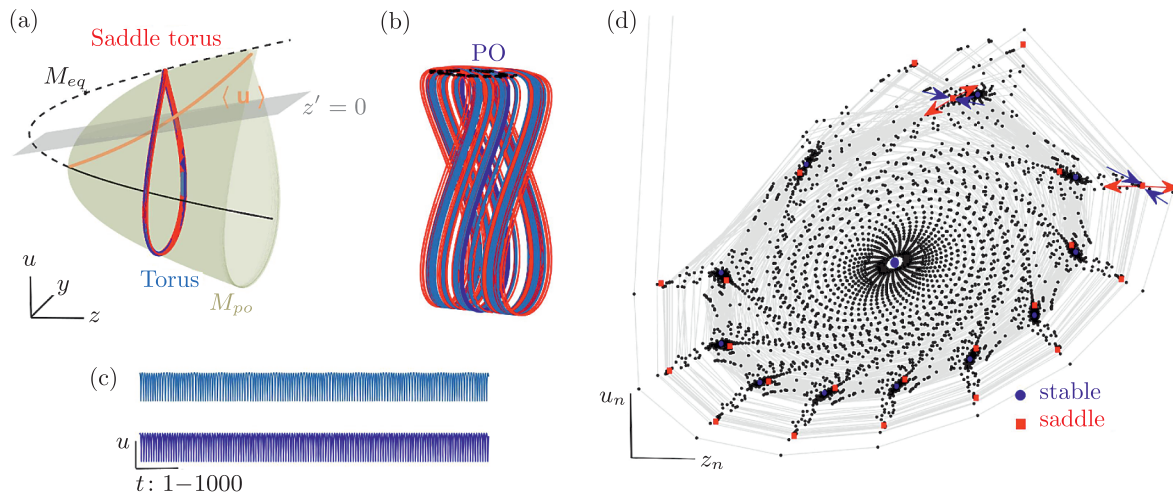

Fig. 6. (a) 3D phase space depicting the bottom sections of the slow-motion manifolds, 1D quiescent manifold M_{eq} and 2D tonic-spiking manifold M_{po}, superimposed with stable tonic-spiking (blue curve), stable quasi-periodic orbits (light blue curve), and saddle torus canard (red curve) at $\eta = 1.102$ and $\bar{u} = -1.35011$ that are highlighted in inset (b). The grey surface $z' = 0$ is the slow nullcline whose intersection with the average curve $\langle u \rangle$ (the orange line) approximates the position of the spiking periodic orbit PO on M_{po}. (c) Time series of spiking and quasi-periodic orbits. (d) Poincaré return maps defined on the maxima of u at $\eta = 1.102$ and $\bar{u} = -1.35011$ achieved by sweeping the initial conditions. The grey lines connect successive iterates, turning counterclockwise in the return map. The stable limit cycle is denoted by blue circles and the saddle one by red squares.

In what follows, we use the first Poincaré return map to analyze the dynamics. We will apply continuation techniques to the Poincaré return maps. The numerical results of the Pernarowski model investigation show that the system is extremely sensitive to the assigned parameters and initial conditions. The saddle torus canard drives the system towards the bursting basin of attraction, rendering continuation methods ineffective in revealing its dynamics. Hence, it is necessary to change the existing initial values in order to stay within the saddle torus. The key to grasping the torus lies in closely monitoring the stable points as we enter its attraction basin.

We decrease $\bar{u}$ on the $\eta = 1.102$ pathway. As shown in Fig. 7, there are four striking spiraling shapes surrounding the stable point. As $\bar{u}$ decreases, its iterates converge clockwise to the stable fixed point with a Floquet multiplier with the imaginary part close to $2\pi/10$ as shown by

the corresponding 10 sleeves at $\bar{u} = -1.34$ (see Fig. 7a). The convergence shape crossing $2\pi/11$ resonance is displayed in Figs. 7B–7C at $\bar{u} = -1.35$ and $\bar{u} = -1.350800944$. At the saddle points, the points accumulate and eventually converge to the stable point at $\bar{u} = -1.35$. A slight decrease in the value of $\bar{u}$ makes the solutions stay close to nested saddle points, shown in Fig. 7c. Figure 7d displays the slow iterates converging to a weakly stable focus at $\bar{u} = -1.3219$. Depending on the conditions or parameter values, the trajectories may shift to bursting, tonic spiking state or resonant tori.
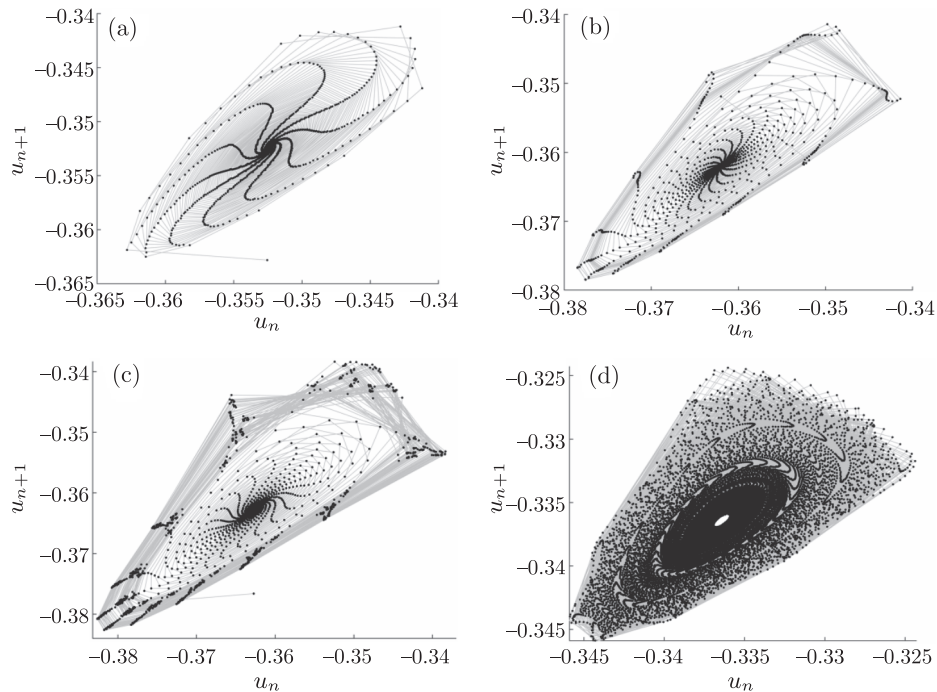
Fig. 7. Torus bifurcations in the 1D Poincaré return map: $u_n \to u_{n+1}$ displaying the maxima of the variable u. The grey lines show connecting successive iterates, which turn counterclockwise. (a) Its iterates converging to a stable fixed point with a Floquet multiplier with the imaginary part close to $\pi/5$ as indicated by the corresponding 10 sleeves of the fixed point at $\bar{u} = -1.34$, next (b) crossing $2\pi/11$ resonance at $\bar{u} = -1.35$, and (c) at $\bar{u} = -1.350800944$. (b) Saddle points corresponding to a saddle orbit lying down on a resonant torus. (c) The situation depicted in inset (c) illustrates that a small decrease in $\bar{u}$ leads to the appearance of nested resonant tori that are self-similar. (d) Inset (d) depicts a slow convergence to a weakly stable focus at $\bar{u} = -1.3219$. We see a multiple resonance convergence that brings out the existence of multiple resonant tori surrounding the stable periodic orbit.

The surrounding stable points exhibit dynamic patterns similar to the original one. The spiral shapes look similar to those presented in Fig. 7, forming self-similar nested resonant tori. Figure 8a displays a regular spiraling when $\bar{u}$ is equal to -1.324794. The system enters a resonance state at $\bar{u} = -1.3262$, (refer to Fig. 8b). Each resonance state is present at nearby saddle points. As $\bar{u}$ increases further, the convergence shapes alternate between ergodic and resonance states.

Further, we sweep the parameter $\bar{u}$ to reveal the dynamics of the fractals. We examine the dynamical rhythms around the fixed points created through a period 8 limit cycle. This torus has appeared through a saddle-node bifurcation. As shown in Fig. 9a, the revolution around stable points is regular for parameter values within the range of $\bar{u} \in (-1.32465, -1.3245)$. We apply a continuation technique on the Poincaré map to extend $\bar{u}$ within the above-mentioned interval. One can observe that the saddle torus canard is far from the resonant torus. Hence, we see a petal shape surrounding the spiking periodic orbit. As the parameter decreases, the system spirals towards the fixed points in a resonant manner. This is demonstrated in Fig. 9b for $\bar{u} \in (-1.32599, -1.32597)$. Here, the torus exhibits two levels of self-similarity. Observations show that fractals are visible when the resonant tori are located extremely close to the saddle torus canard. Several resonant tori with
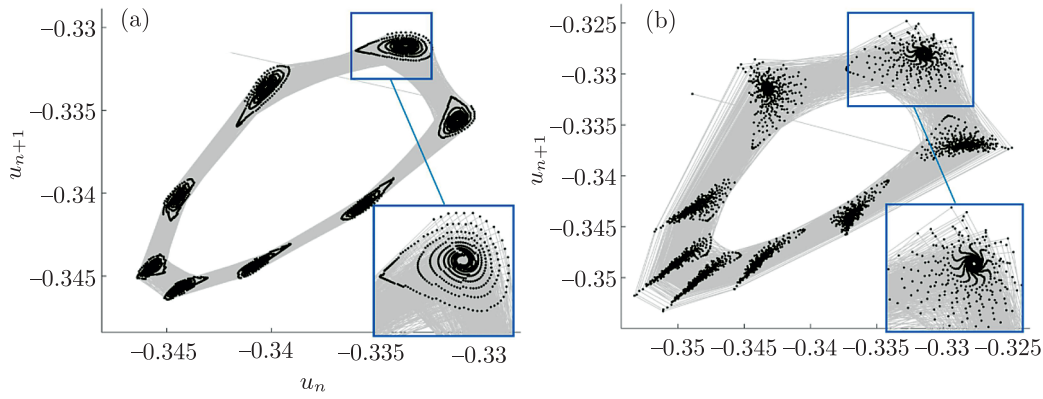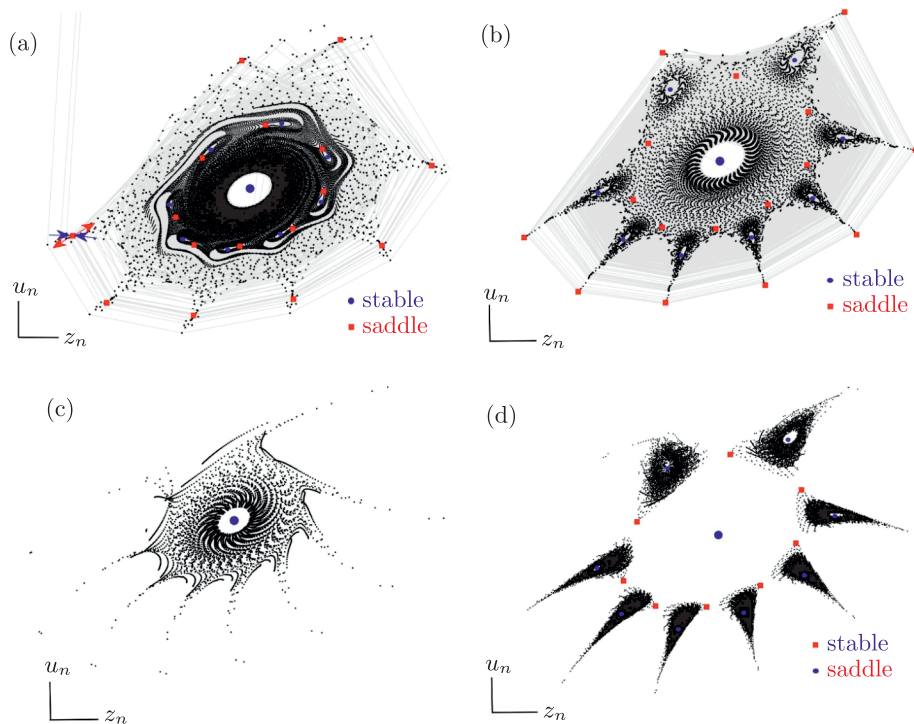
Fig. 8. A stable 1:8-resonant torus at $\eta = 1.102$. (a) The period-8 stable points on the Poincaré return map defined on the maxima of u show regular convergence. Inset (a) shows the torus at $\bar{u} = -1.324794$ due to the loss of smoothness after the multipliers of the stable periodic points become complex conjugate, soon followed by the formation of homoclinic curves of the saddle ones in between as indicated by a sharp angle of the converging spiral in the inset. (b) Similar dynamics at $\bar{u} = -1.3262$ with a weaker convergence to the stable periodic orbit depicting self-similarity in some range of $\bar{u}$. Here, the grey lines connect successive iterates, turning counterclockwise in the return map.

different periods can coexist in intriguing situations. However, the fractals are the closest to the torus canard. Figure 9c shows a nine-prong star in the Poincaré return maps, where the original stable point is a resonant focus in the parameter range $\bar{u} \in (-1.3366, -1.3356)$. Star prongs formation is due to the presence of saddles that impress a convergence or divergence shape. It is interesting to note that star prongs appear near each fixed point within the range of $\bar{u} \in (-1.3262, -1.3259)$ as shown in Fig. 9d. Figure 9 depicts two levels of self-similarity observed in the fractal of nested resonant tori.

5. QUASI-PERIODICITY THROUGH TORUS BREAK-DOWN

The model behavior is richer and more complex near the torus bifurcation. Several windows of phase-locking appear when the parameter alters within the torus bifurcation interval. As the parameter increases, the small spiking periodic-orbit becomes quasi-periodic through a torus bifurcation. The system remains multistable, with multiple tori and bursting. Different tori include a stable ergodic torus and several resonant tori. The new born torus is ergodic first: then it grows up and breaks down through a homoclinic to a saddle bifurcation. Then the system will either converge to a resonant torus or approach to the bursting, depending on the initial conditions. Figure 10 shows four pivotal stages from torus onset until its break-down on the pathway $\eta = 1.102$. This figure shows parameter situations in which the torus is ergodic (part (a) at $\bar{u} = -1.321093$), and also shows a situation where the torus deforms (insets (b)–(c) at $\bar{u} = -1.321092, \bar{u} = -1.3210919$), getting close to the seven saddle points corresponding to a period-7 saddle periodic orbit, or the situation where the torus has already collided with the saddles (d). The pathway can exhibit a resonance torus with period 28, as depicted in Fig. 10d.

Figure 11 displays a gallery of invariant circles that correspond to the growth of the ergodic stable torus emerging from a stable periodic orbit at (a) $\eta = 1.102$ and (b) $\eta = 1.07$. The torus is smooth first and becomes nonsmooth later, coming close to the saddle points. Then it breaks down. The collision with a period 4 saddle resonant torus leads to torus destruction at $\eta = 1.07$. The Poincaré map in Fig. 12 displays the saddle points as red squares outside the ergodic torus. The existence of saddle points is established by continuing in the initial values of u of the Pernarowski system. As shown in the figure, the trajectories at the saddle tori can either approach a stable torus or escape towards large scale (stable) bursting oscillations along the unstable manifolds (or set) of the resonant saddle periodic orbits on the invariant circle. One can verify the approach of the ergodic torus to the saddle by observing the time that the system spends at each part of the

Fig. 9. Evolution of stable resonant tori in the 2D Poincaré return maps generated by solutions of the Pernarowski model on the $\eta = 1.102$ pathway. (a) A stable 1:8-resonant torus appears by a saddle-node bifurcation at $\bar{u} \simeq -1.326$, where it is located far away from the saddle torus canard. The red squares in the Poincaré map correspond to saddle tori, whereas blue circles relate to stable periodic orbits. Grey lines are used to show the movement of the trajectories between points. A regular convergence toward the stable points gets a petal shape for parameter values in the interval $\bar{u} \in (-1.32465, -1.3245)$. The original stable point has regular spiraling. (b) Inset B shows two levels of self-similarity observed in the fractal decreasing $\bar{u}$ in the interval $(-1.32599, -1.32597)$. We see that the fractal is located near the saddle torus canard. Also, the original stable point exhibits resonant spiraling. (c) A nine-prong star continuing $\bar{u} \in (-1.3366, -1.3356)$. (d) Similar stars near the stable points on the tori at $\bar{u} \in (-1.3262, -1.3259)$.

torus. As the torus becomes more destroyed, the trajectories spend more time in the vicinity of the saddles. The authors in [23] reported the same scenario for torus destruction.

The system's behavior is richer in the $\eta = 1.102$ pathway. KAM tori, a resonant torus together with self-similar nested resonant tori, are surrounding the ergodic torus. Despite its dissipative nature, this system exhibits a curious phenomenon with the coexistence of KAM tori and a fractal. Here, a feature of integrable Hamiltonian systems is present in dissipative systems. Each invariant set competes with others, capturing its attraction basin, so the system is sensitive to initial conditions. The ergodic torus is smooth first. It becomes nonsmooth, reaching seven saddle points on the KAM tori. Then it collides with the saddles and breaks down. The closer the torus approaches the saddles, the more the time the trajectories spend near the torus corners. Figure 12a shows the dynamics. We display the saddles (red squares) and the routes that depart from the saddles and return to them close to their unstable manifolds. Suitable initial conditions cause the placement of resonant and self-similar tori around the ergodic torus.

The self-similar nested resonant torus shown in Fig. 12a has appeared before the torus bifurcation, so it coexists with the spiking periodic orbit. As stated, the behavior of the nested fixed points is similar to that of the original point. Each node becomes repelling, forming a nested ergodic torus when $\bar{u}$ increases near the torus bifurcation. The new torus follows a similar pathway as the original one from its onset to its break-down. A typical evolution of the nested ergodic and resonant torus is illustrated in Fig. 13, altering $\bar{u}$ in the interval $(-1.321107, -1.32106)$, which reveals an intriguing phenomenon occurring near the nested tori. The convergence to the fixed points is slow near the torus bifurcation occurring at $\bar{u} = -1.321107$ as illustrated by Fig. 13b. The
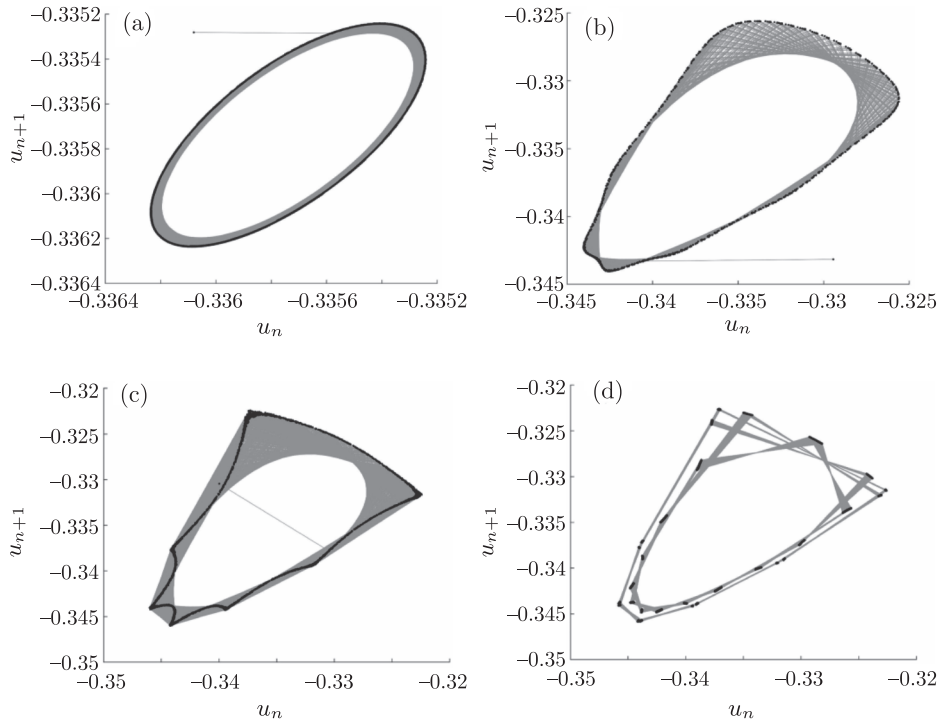
Fig. 10. Pivotal stages depicting different stages from the ergodic stable torus emergence until its break-down on the $\eta = 1.102$ pathway. Inset (a) shows the Poincaré map defined on the maximum values of u just near the torus bifurcation at $\bar{u} = -1.321093$, where an ergodic torus appears. The grey lines connect successive iterates, turning counterclockwise in the return map. (b)–(c) The torus grows up and deforms, getting close to the seven saddle points corresponding to a period-7 unstable saddle orbit at $\bar{u} = -1.321092$, $\bar{u} = -1.3210919$. (d) A resonant torus surrounding the ergodic torus. Destroying the torus causes the system to approach a resonant torus around it or go towards the bursting relying on initial conditions.

fixed points become repelling and form a nested ergodic torus that starts out smooth but becomes nonsmooth. It then breaks down like the original torus. Nested saddle points seem to have affected the smoothness of each resonant torus.

Figure 14 shows a bifurcation diagram displaying the Poincaré return maps of the consecutive maxima of u sweeping $\bar{u}$ at $\eta = 1.102$. The thin line in the diagram shows the dynamical regimes near the periodic orbit and the ergodic torus after it appears from the torus bifurcation. Multiple branches highlighted in Fig. 14a correspond to a resonant torus. The earlier emerging torus grows and breaks down suddenly to a large amplitude bursting oscillation on the right. Here, a KAM torus surrounds the stable ergodic torus. Two sets of saddle points encircle the new torus. Also, a self-similar nested resonant torus, together with another resonant torus, is located there. In Fig. 12a, we examined this scenario. The switching mechanism in the left part of Fig. 14a is due to the saddle torus canard, although the self-similar torus covers the periodic orbit. As the parameters vary, the trajectories fall into the attraction basin of the bursting to manifest burst oscillations. Several points below and above the thin line in Fig. 14 refer to symmetric bursting orbits. Bursting oscillations can be stable if their branches are uninterrupted. They can be chaotic, entering regions where the number of spikes increases through period-doubling bifurcations. Figure 14b depicts several spike-adding mechanisms in the bursting oscillations. To the left of the thin line, the Pernarowski model also produces large-amplitude bursting oscillations. The trajectories pursue the unstable manifolds of the saddles to leave towards the chaotic bursting. Figure 14 shows a transient route between chaotic and regular bursting.

6. BLUE-SKY CATASTROPHE

Next, we consider the $\eta = 2$ pathway. Figure 15 depicts the slow-motion manifolds comprising 2D tonic-spiking manifolds and a 1D quiescent one. The tonic spiking starts with a subcritical
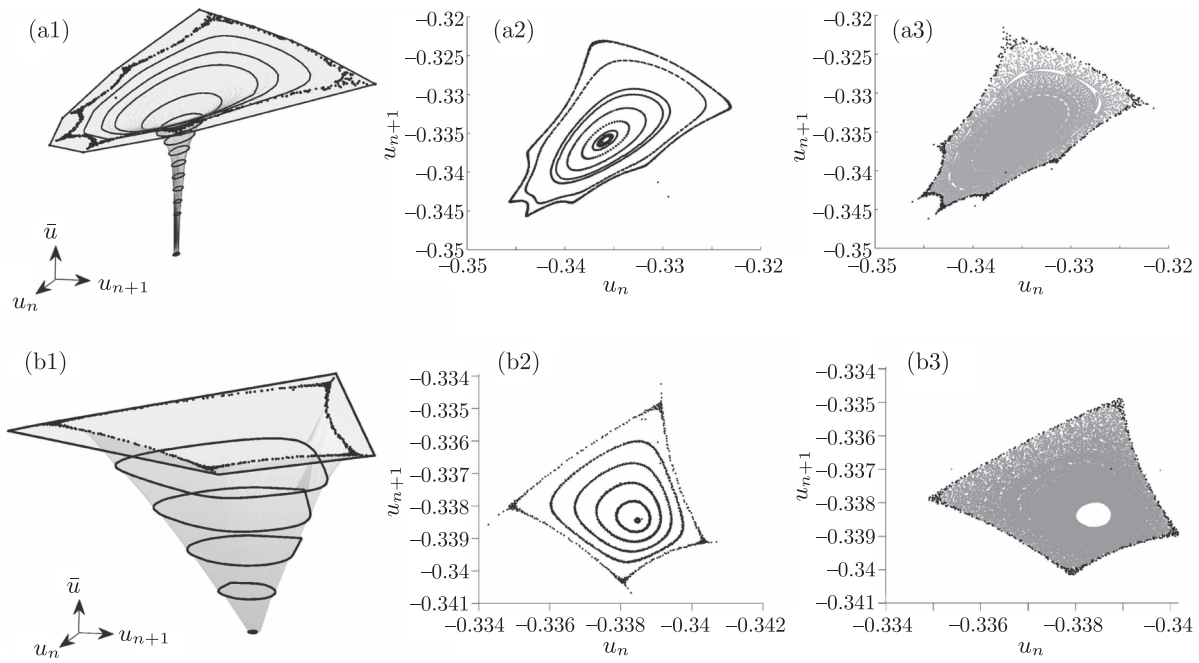
Fig. 11. Evolution of a stable invariant curve (resp. a stable torus) in the 1D Poincaré return map $T : u_{\max}^n \to u_{\max}^{n+1}$ as $\bar{u}$ increases from -1.321093 through -1.3210919 at $\eta = 1.102$ in Panels A and from -1.281 through -1.28 at $\eta = 1.07$ in panels B. (A2-3) A smooth round circle increases in size and becomes nonsmooth with a weak resonance. (B2-3) It quickly becomes of a "square-shape" form corresponding to a stable 1:4 resonant torus in the Pernarowski model.
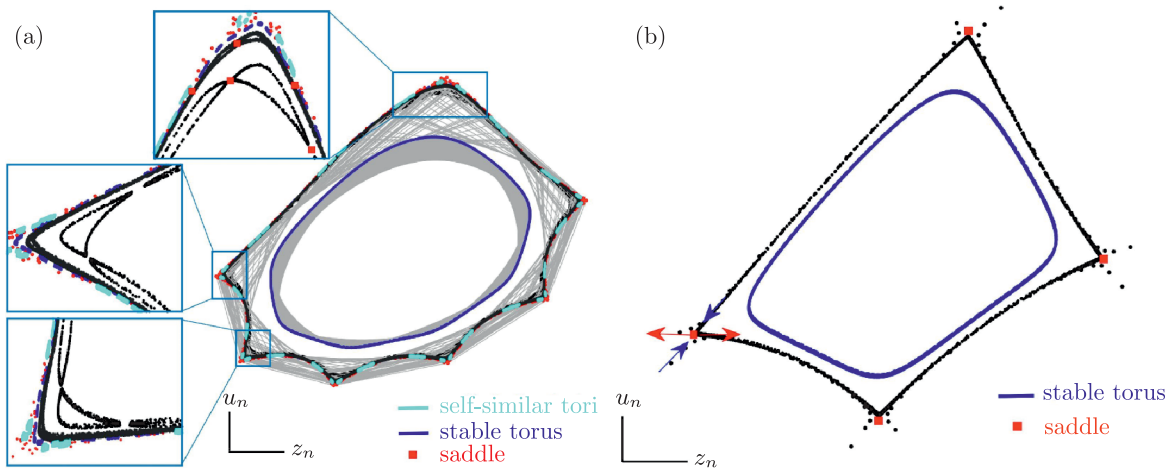
Fig. 12. Poincaré return maps defined on the consecutive maxima of u at $\eta = 1.102$, $\bar{u} = -1.321092$ in panel A and at $\eta = 1.07$, $\bar{u} = -1.2805$ in panel B. (a) An invariant KAM torus [29] coexisting with a stable resonant torus (blue curve), self-similar resonant tori (turquoise blue), and a saddle torus canard (red curve) surrounds the ergodic torus; the torus grows and breaks down, colliding with the saddle points. In the return map, successive iterates are connected by grey lines that turn counterclockwise. (b) A square-shape stable torus (blue curve) grows in size and breaks down, reaching the saddle torus canard (red curve).

Hopf bifurcation, where a repelling periodic orbit emerges. The periodic orbit gets stable through a fold bifurcation and then loses its stability by a torus bifurcation. Then it becomes stable with the second torus bifurcation. This manifold draws back off (green branch), so that its stable part (not represented here) ends with another torus bifurcation on the right. The purple line depicts the average curve of the tonic-spiking manifold. A torus bifurcation occurs after the collision of the slow nullcline with the purple line at its fold, resulting in the creation of a stable periodic orbit
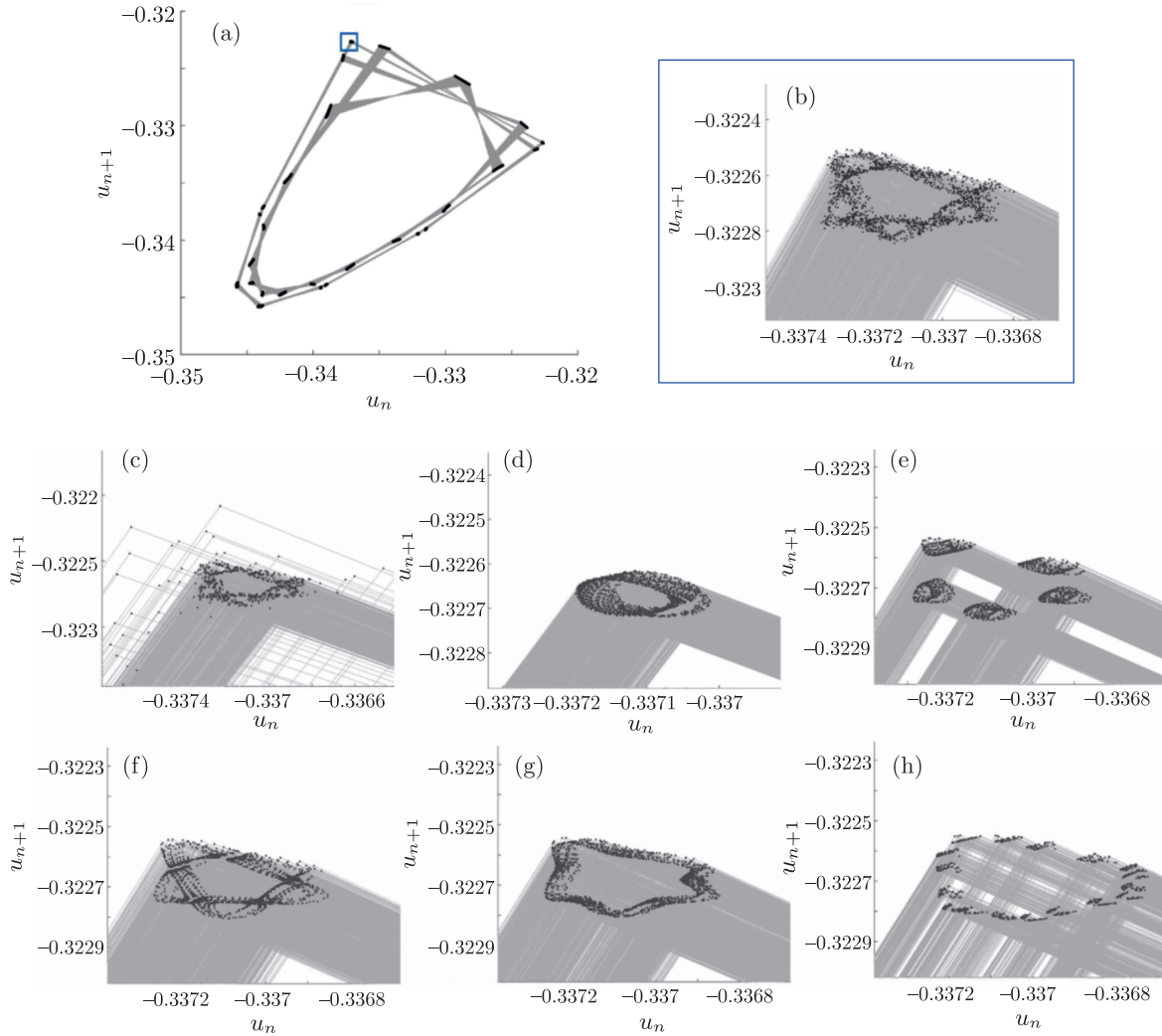
Fig. 13. Typical evolution of dynamical regimes in the indicated box on the self-similar tori varying $\bar{u} \in (-1.321107, -1.32106)$. (b) weakly convergence towards the stable points on the tori at $\bar{u} = -1.321107$, where the torus bifurcation has not occurred. (c) Saddle torus canard is the switching mechanism towards the bursting at $\bar{u} = -1.3211$. (d) Inset (d) shows the emergence of a nested stable ergodic torus at $\bar{u} = -1.321097$, where the torus bifurcation has occurred. Insets (e)–(h) represent a different evolution of the dynamical regimes in the indicated box, increasing $\bar{u}$. The grey lines indicate the movement of the trajectories between the points on the map.

with a large amplitude from a stable torus. The stability of the torus is due to the fact that, on average, the trajectories spend more time on the stable branch of M_{po} than on the unstable one. As η decreases, the torus bifurcation at the fold is replaced with a fold bifurcation, so the stable periodic orbit loses its stability to a bursting. When the slow nullcline collides with the fold point near the saddle-node periodic orbit, the trajectories are captured and the limit cycle period and the amplitude increase. This induces a peculiar bifurcation, called the *blue-sky catastrophe*, that leads to long spiking in bursting activities. The blue-sky catastrophe is a codimension-one bifurcation that describes a reversible and continuous transition between bursting and spiking [14, 26, 27, 37–39]. Figure 16 represents this scenario in the $\eta = 1.6$ pathway at $\bar{u} = -0.00499$. The resulting torus is irregular and persists as the saddle-node periodic orbit disappears.

As before, we use the phase portrait of the system to reveal the slow-motion manifolds topology and the slow nullcline $z' = 0$. When the nullcline is slightly below its location shown in Figs. 15 and 16, there will be a stable limit cycle on M_{po}. As the nullcline shifts up, the stable limit cycle approaches the fold where its stability is lost through a fold bifurcation (Fig. 16) or a supercritical
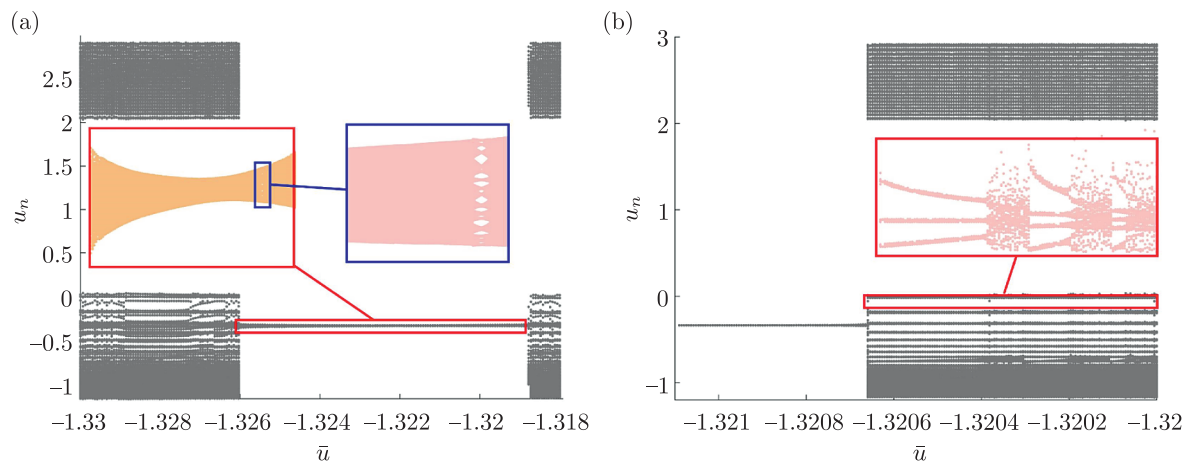
Fig. 14. Poincaré return map of the consecutive maxima of u with fixed initial conditions on the $\eta = 1.102$ pathway. (a) The thin line corresponds to the dynamical regimes around the periodic orbit. The highlighted multiple branches correspond to a resonant torus state. The dense points on the line correspond to various convergence shapes before the torus bifurcation. They resemble the ergodic tori after its occurrence. On the right side the switching mechanism is due to the homoclinic to a saddle bifurcation. The switching mechanism in the left part of Fig. 14a is due to the saddle torus canard. (b) The number of revolutions at each burst increases through cascades of period-doubling bifurcations.

torus bifurcation (Fig. 15). The trajectories oscillate between stable and unstable portions of M_{po} near the fold. Since they linger (on average) longer on the stable branch rather than on the unstable one, each of the regular (Fig. 15) and deformed (Fig. 16) tori is stable. The system shows bursting oscillations, as the torus breaks down by further shifting up the slow nullcline.
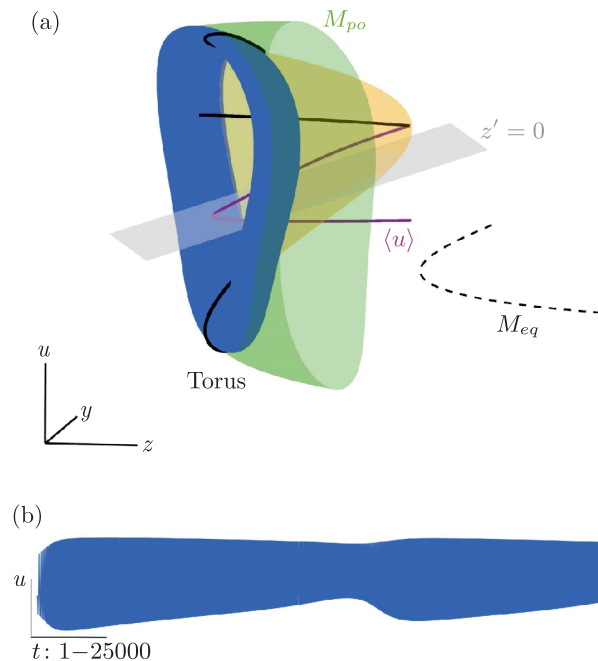
Fig. 15. (a) The phase portrait of the system on the $\eta = 2$ pathway shows a stable torus (blue line) on the fold of the spiking manifold, M_{po}, overlaid on the slow nullcline, $z' = 0$, and the quiescent manifold, M_{eq}. The Poincaré section transversal to the torus at its top and bottom highlights two stable circles (black circles). The purple line $\langle u \rangle$ is the average curve whose intersection with the slow nullcline determines the location of the unstable periodic orbit at the torus bifurcation point. (b) Modulated time series corresponding to the torus in (a).
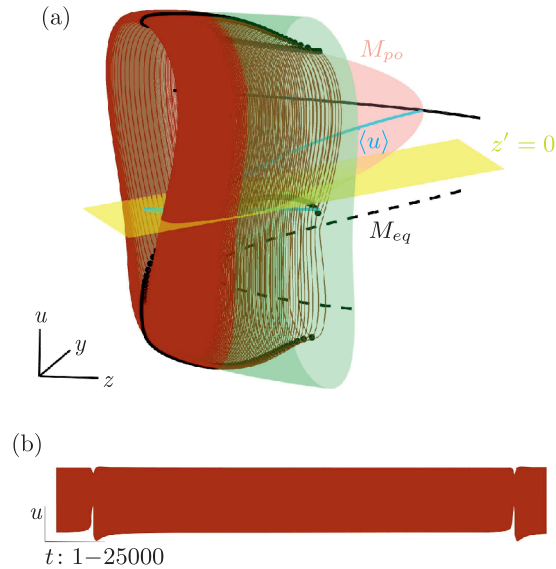
Fig. 16. (a) The phase portrait of the system on the $\eta = 1.6$ pathway shows the blue-sky catastrophe (brown curve) on the fold of the spiking manifold, M_{po}, overlaid on the slow nullcline, $z' = 0$, and the quiescent manifold, M_{eq}. The Poincaré section transversal to the orbit at its top and bottom highlights two broken circles (black circles). The blue line $\langle u \rangle$ is the average curve whose intersection with the slow nullcline finds the location of the saddle-node periodic orbit at the fold of M_{po}. (b) Modulated time series corresponding to the orbit in (a).

With further decrease in $\eta < 1.5$, the outer branch of the tonic-spiking manifold splits into two branches, colliding with the quiescent manifold by a homoclinic bifurcation. The inwards branch shrinks near the Hopf point on the quiescent manifold. At about $\eta = 1.2$, both inner homoclinic bifurcations occur at the same saddle point. This was shown in Fig. 1 as evidence of a blue-sky catastrophe.

7. DISCUSSION AND FUTURE RESEARCH

In this study, we have examined the Pernarowski system, focusing on global bifurcations that lead to quasi-periodicity and blue-sky catastrophe. Our exploration involves a range of torus bifurcations, including a supercritical torus bifurcation, a saddle torus canard, a resonant torus, self-similar nested resonant tori, torus destruction, and invariant KAM tori. At the transition route from bursting to spiking, the blue-sky catastrophe occurs.

Beta cells experience burst activities which are categorized into fast, medium, and slow bursts [40–44]. Slow burst activities are distinguished by their extended periods compared with medium or fast bursts. Our interest lies in the mechanisms that result in slow burst observations. The homoclinic bifurcation to a saddle point may explain the mechanism of these oscillations [44]. We expect to use the blue-sky catastrophe observed in the Pernarowski model as a foundation to comprehend such scenarios and to propose an avenue for future research.

Besides, we have found a proof of torus and successive period-doubling (flip) bifurcations in this model. The recent study [36] has demonstrated that the existence and location of these bifurcations set physiological boundaries for ion gradient variation, affecting membrane voltage sensitivity and simulation variability. Physiological models of beta cells will investigate the ion gradient bounds by analyzing the torus and consecutive flip bifurcations.

8. CONCLUSION

We have considered and analyzed the Pernarowski model describing bursting activities in pancreatic beta cells, which features torus bifurcations on the tonic-spiking manifolds. In the model, we have shown kinds of stable, resonant, saddle torus canard, and KAM tori. The question of

determining the stability of a torus through a torus bifurcation is a complicated problem compared to the canard appearing in 2D systems whose stability can be determined by the properties of the functions on the right side. To prove the existence of a saddle torus canard, we employed the Poincaré return map of the maximum values of the variable u and the parameter sweep algorithm to find two initial conditions for which one trajectory goes inside the torus to approach the nested stable periodic orbit or stable torus, while the other trajectory converges to the other attractor. This proves the existence of a saddle torus. Although continuation software, such as MATCONT, applies to detect torus bifurcations, it is inadequate in analyzing resonant torus bifurcations and torus break-downs. A Poincaré return map is a rigorous tool for analyzing dynamics in such situations.

Our approach illustrates the coexistence of resonant and KAM tori as well as the self-similarity of nested resonant tori around a stable periodic orbit, resulting from fold or inverse period-doubling bifurcations. Through torus bifurcation, we have found that a stable node can produce a stable torus, which starts out smooth and becomes nonsmooth, converging with existing saddle points. There is evidence that a similar phenomenon occurs around the nested newborn tori. Here, an intriguing phenomenon is the occurrence of multistability involving the coexistence of multiple resonant tori, and invariant KAM tori in the Pernarowski model which is a dissipative system. These phenomena are typically seen in integrable Hamiltonian systems, but also occur in dissipative systems.

We would like to highlight that we have applied an alternative method that examines the system behavior by utilizing critical slow-motion manifolds of the full model rather than the fast subsystem. By using the average curve, we studied the dynamics in the vicinity of a tonic-spiking manifold. This approach allowed us to uncover evidence of blue-sky catastrophe in the Pernarowski model. Torus and period-doubling bifurcations resulted in the loss of stability of the periodic orbit in the model considered. The recent work [36] reported that the location and existence of these bifurcations act as physiological limits on ion gradient variability and might affect the frequency and the shape of neural mass spiking rhythms.

ACKNOWLEDGMENTS

CONFLICT OF INTEREST

The authors declare that they have no conflict of interest.

PUBLISHER'S NOTE

Pleiades Publishing remains neutral with regard to jurisdictional claims in published maps and institutional affiliations.

REFERENCES

1. Ashcroft, F. and Rorsman, P., Electrophysiology of the Pancreatic Beta-Cell, *Prog. Biophys. Mol. Biol.,* 1989, vol. 54, no. 2, pp. 87–143.
2. Chay, T. R. and Keizer, J., Minimal Model for Membrane Oscillations in the Pancreatic Beta-Cell, *Biophys. J.,* 1983, vol. 42, no. 2, pp. 181–190.
3. Chay, T. R., Glucose Response to Bursting-Spiking Pancreatic β-Cells by a Barrier Kinetic Model, *Biol. Cybern.,* 1985, vol. 52, no. 5, pp. 339–349.
4. Chay, T. R. and Rinzel, J., Bursting, Beating, and Chaos in an Excitable Membrane Model, *Biophys. J.,* 1985, vol. 47, no. 3, pp. 357–366.
5. Pernarowski, M., Miura, R. M., and Kevorkian, J., The Sherman – Rinzel – Keizer Model for Bursting Electrical Activity in the Pancreatic β-Cell, in *Differential Equations Models in Biology, Epidemiology and Ecology,* S. Busenberg, M. Martelli (Eds.), Lecture Notes in Biomath., vol. 92 Berlin: Springer, 1991, pp. 34–53.

6. Han, K., Kang, H., Kim, J. and Choi, M., Mathematical Models for Insulin Secretion in Pancreatic β-Cells, *Islets,* 2012, vol. 4, no. 2, pp. 94–107.

7. Felix-Martínez, G. J. and Godínez-Fernández, J. R., Mathematical Models of Electrical Activity of the Pancreatic β-Cell: A Physiological Review, *Islets,* 2014, vol. 6, no. 3, e949195, 14 pp.

8. FitzHugh, R., Impulses and Physiological States in Theoretical Models of Nerve Membrane, *Biophys. J.,* 1961, vol. 1, no. 6, pp. 445–466.

9. Hindmarsh, J. L. and Rose, R. M., A Model of Neuronal Bursting Using Three Coupled First Order Differential Equations, *Proc. R. Soc. Lond. Ser. B Biol. Sci.,* 1984, vol. 221, no. 1222, pp. 87–102.

10. de Vries, G., Multiple Bifurcations in a Polynomial Model of Bursting Oscillations, *J. Nonlinear Sci.,* 1998, vol. 8, no. 3, pp. 281–316.

11. Izhikevich, E. M., Neural Excitability, Spiking and Bursting, *Internat. J. Bifur. Chaos Appl. Sci. Engrg.,* 2000, vol. 10, no. 6, pp. 1171–1266.

12. Izhikevich, E. M., *Dynamical Systems in Neuroscience: The Geometry of Excitability and Bursting,* Cambridge, Mass.: MIT Press, 2007.

13. Fallah, H., Symmetric Fold/Super-Hopf Bursting, Chaos and Mixed-Mode Oscillations in Pernarowski Model of Pancreatic β-Cells, *Internat. J. Bifur. Chaos Appl. Sci. Engrg.,* 2016, vol. 26, no. 9, 1630022, 14 pp.

14. Shilnikov, A. and Cymbalyuk, G., Transition between Tonic Spiking and Bursting in a Neuron Model via the Blue-Sky Catastrophe, *Phys. Rev. Lett.,* 2005, vol. 94, no. 4, 048101, 4 pp.

15. Terman, D., The Transition from Bursting to Continuous Spiking in Excitable Membrane Models, *J. Nonlinear Sci.,* 1992, vol. 2, no. 2, pp. 135–182.

16. Tsaneva-Atanasova, K., Osinga, H. M., Rieß, Th., and Sherman, A., Full System Bifurcation Analysis of Endocrine Bursting Models, *J. Theoret. Biol.,* 2010, vol. 264, no. 4, pp. 1133–1146.

17. Kuznetsov, A. P., Kuznetsov, S. P., and Stankevich, N. V., A Simple Autonomous Quasiperiodic Self-Oscillator, *Commun. Nonlinear Sci. Numer. Simul.,* 2010, vol. 15, no. 6, pp. 1676–1681.

18. Shilnikov, A., Calabrese, R. L., and Cymbalyuk, G., Mechanism of Bistability: Tonic Spiking and Bursting in a Neuron Model, *Phys. Rev. E (3),* 2005, vol. 71, no. 5, 056214, 9 pp.

19. Shilnikov, A. and Kolomiets, M., Methods of the Qualitative Theory for the Hindmarsh – Rose Model: A Case Study. A Tutorial, *Internat. J. Bifur. Chaos Appl. Sci. Engrg.,* 2008, vol. 18, no. 8, pp. 2141–2168.

20. Kramer, M. A., Traub, R. D., and Kopell, N. J., New Dynamics in Cerebellar Purkinje Cells: Torus Canards, *Phys. Rev. Lett.,* 2008, vol. 101, no. 6, 068103, 4 pp.

21. Afraimovich, V. S. and Shilnikov, L. P., Certain Global Bifurcations Connected with the Disappearance of a Fixed Point of Saddle-Node Type, *Dokl. Akad. Nauk SSSR,* 1974, vol. 219, pp. 1281–1284 (Russian).

22. Ju, H., Neiman, A. B., and Shilnikov, A. L., Bottom-Up Approach to Torus Bifurcation in Neuron Models, *Chaos,* 2018, vol. 28, no. 10, 106317, 21 pp.

23. Pereira, T., Baptista, M. S., Reyes, M. B., Caldas, I. L., Sartorelli, J. C., and Kurths, J., A Scenario for Torus T^2 Destruction via a Global Bifurcation, *Chaos Solitons Fractals,* 2009, vol. 39, no. 5, pp. 2198–2210.

24. Channell, P., Jr., Cymbalyuk, G., and Shilnikov, A., Applications of the Poincaré Mapping Technique to Analysis of Neuronal Dynamics, *Neurocomputing,* 2007, vol. 70, nos. 10–12, pp. 2107–2111.

25. Channell, P., Cymbalyuk, G., and Shilnikov, A., Origin of Bursting through Homoclinic Spike Adding in a Neuron Model, *Phys. Rev. Lett.,* 2007, vol. 98, no. 13, 134101, 4 pp.

26. Cymbalyuk, G. and Shilnikov, A., Coexistence of Tonic Spiking Oscillations in a Leech Neuron Model, *J. Comput. Neurosci.,* 2005, vol. 18, no. 3, pp. 255–263.

27. Shilnikov, L. P., Shilnikov, A. L., Turaev, D., and Chua, L. O., *Methods of Qualitative Theory in Nonlinear Dynamics: Part 1,* World Sci. Ser. Nonlinear Sci. Ser. A Monogr. Treatises, vol. 4, River Edge, N.J.: World Sci., 1998.
Shilnikov, L. P., Shilnikov, A. L., Turaev, D., and Chua, L. O., *Methods of Qualitative Theory in Nonlinear Dynamics: Part 2,* World Sci. Ser. Nonlinear Sci. Ser. A Monogr. Treatises, vol. 5, River Edge, N.J.: World Sci., 2001.

28. Shilnikov, A., Complete Dynamical Analysis of a Neuron Model, *Nonlinear Dynam.,* 2012, vol. 68, no. 3, pp. 305–328.

29. Arnol'd, V. I., Small Denominators and Problems of Stability of Motion in Classical and Celestial Mechanics, *Russian Math. Surveys,* 1963, vol. 18, no. 6, pp. 85–191; see also: *Uspekhi Mat. Nauk,* 1963, vol. 18, no. 6(114), pp. 91–192.

30. Arnol'd, V. I., Proof of a Theorem of A. N. Kolmogorov on the Invariance of Quasi-Periodic Motions under Small Perturbations of the Hamiltonian, *Russian Math. Surveys,* 1963, vol. 18, no. 5, pp. 9–36; see also: *Uspekhi Mat. Nauk,* 1963, vol. 18, no. 5, pp. 13–40.

31. Calleja, R., Celletti, A., and de la Llave, R., KAM Theory for Some Dissipative Systems, in *New Frontiers of Celestial Mechanics: Theory and Applications,* G. Baù, S. Di Ruzza, R. I. Páez, T. Penati, M. Sansottera (Eds.), Springer Proc. Math. Stat., vol. 399, Cham: Springer, 2022, pp. 81–122.

32. Kolmogorov, A. N., Théorie générale des systèmes dynamiques et mécanique classique, in *Proc. of the Internat. Congr. of Mathematicians (Amsterdam, 1954): Vol. 1,* Groningen: Noordhoff, 1957, pp. 315–333.

33. de Vries, G. and Miura, R. M., Analysis of a Class of Models of Bursting Electrical Activity in Pancreatic β-Cells, *SIAM J. Appl. Math.,* 1998, vol. 58, no. 2, pp. 607–635.

34. Pernarowski, M., Fast and Slow Subsystems for a Continuum Model of Bursting Activity in the Pancreatic Islet, *SIAM J. Appl. Math.,* 1998, vol. 58, no. 5, pp. 1667–1687.

35. Pernarowski, M., The Mathematical Analysis of Bursting Electrical Activity in Pancreatic β-Cells, *PhD Dissertation,* Univ. of Washington, Seattle, Wash., 1990, 332 pp.

36. Chesebro, A. G., Mujica-Parodi, L. R., and Weistuch, C., Ion Gradient-Driven Bifurcations of a Multi-Scale Neuronal Model, *Chaos Solitons Fractals,* 2023, vol. 167, Paper No. 113120, 8 pp.

37. Shil'nikov, L. P. and Turaev, D. V., On Simple Bifurcations Leading to Hyperbolic Attractors, *Comput. Math. Appl.,* 1997, vol. 34, nos. 2–4, pp. 441–457.

38. Shilnikov, L. P. and Turaev, D. V., A New Simple Bifurcation of a Periodic Orbit of "Blue Sky Catastrophe" Type, in *Methods of Qualitative Theory of Differential Equations and Related Topics,* Amer. Math. Soc. Transl. Ser. 2, vol. 200, Providence, R.I.: AMS, 2000, pp. 165–188.

39. Shilnikov, A. L., Shilnikov, L. P., and Turaev, D. V., On Some Mathematical Topics in Classical Synchronization: A Tutorial, *Internat. J. Bifur. Chaos Appl. Sci. Engrg.,* 2004, vol. 14, no. 7, pp. 2143–2160.

40. Beauvois, M. C., Merezak, Ch., Jonas, J.-Ch., Ravier, M. A., Henquin, J.-C., and Gilon, P., Glucose-Induced Mixed $[Ca^{2+}]$ Oscillations in Mouse β-Cells Are Controlled by the Membrane Potential and the SERCA3 Ca^{2+}-ATPase of the Endoplasmic Reticulum, *Am. J. Physiol. Cell. Physiol.,* 2006, vol. 290, no. 6, pp. C1503–C1511.

41. Kinard, T. A., de Vries, G., Sherman, A., and Satin, L. S., Modulation of the Bursting Properties of Single Mouse Pancreatic β-Cells by Artificial Conductances, *Biophys. J.,* 1999, vol. 76, no. 3, pp. 1423–1435.

42. Smith, P. A., Ashcroft, F. M., and Rorsman, P., Simultaneous Recordings of Glucose Dependent Electrical Activity and ATP Regulated K^{+}-Currents in Isolated Mouse Pancreatic β-Cells, *Fed. Eur. Biochem. Soc. Lett.,* 1990, vol. 261, no. 1, pp. 187–190.

43. Zhang, M. Goforth, P., Bertram, R., Sherman, A., and Satin, L., The Ca^{2+} Dynamics of Isolated Mouse β-Cells and Islets: Implications for Mathematical Models, *Biophys. J.,* 2003, vol. 84, no. 5, pp. 2852–2870.

44. Fazli, M., Vo, Th., and Bertram, R., Phantom Bursting May Underlie Electrical Bursting in Single Pancreatic β-Cells, *J. Theor. Biol.,* 2020, vol. 501, 110346, 14 pp.